Contribution from the Fachbereich Chemie, Philipps-Universität, D-3550 Marburg, FRG, and Institut für Anorganische Chemie der Universität, D-5300 Bonn, FRG

Single-Crystal EPR and Optical Absorption Investigations of the Ozonide Radical in Crystalline Solids MO_3 ($M = K^+$, Rb^+, Cs^+, $N(CH_3)_4^+$, $N(C_2H_5)_4^+$)†

G. Steffen,‡ W. Hesse,§ M. Jansen,§ and D. Reinen*,‡

Received March 14, 1990

The orientation and magnitudes of the g-tensor components were investigated by single-crystal EPR spectroscopy for the ozonide radical anion in compounds MO_3 (M = K, Rb, Cs, $N(CH_3)_4$, $N(C_2H_5)_4$). The molecular g-values for $N(CH_3)_4O_3$ are $g_x = 2.007$ (2), $g_y = 2.017$ (1), and $g_z = 2.009$ (2) (298 K) with g_x parallel to the *b* axis, g_y parallel to the *a* axis, and g_z parallel to the *c* axis. They do not depend on the counterion M^+ within the experimental error limits. g_z follows the C_2 axis of the bent O_3^- entity of C_{2v} symmetry, while g_x has the direction of the normal to the O_3^- plane. Exchange-narrowed *g* values are found in case of smaller M cations (Rb^+, K^+). The dipolar broadening of the EPR signals is evaluated for the O_3^- radical in the various ozonides by calculating the second moments M_2[d] and comparing with the observed line width, in order to estimate the contributions due to exchange narrowing. Two bands at ≈8000 and ≈18 500 cm^{-1} are observed in the unpolarized single-crystal spectra of KO_3, RbO_3, and $N(CH_3)_4O_3$, again with no significant variation in dependence on the M^+ cation. The lower energy band, which was not observed before, is assigned to the $^2B_1 \rightarrow {}^2A_1$ transition, and the higher energy band, to the $^2B_1 \rightarrow {}^2A_2$ transition. The color, varying from brownish red (KO_3) to orange red ($N(CH_3)_4O_3$), is due to the minimum around 14 000 cm^{-1} and the transparent region above 22 000 cm^{-1}.

Introduction

In recent years single crystals of ozonides MO_3 with alkali-metal and tetraalkylammonium counterions have been prepared and the structures determined.[1-5] One aim of this paper is to investigate these compounds by means of EPR and optical spectroscopy, in order to characterize the geometry and the bonding properties by independent methods. The O_3^- ion has C_{2v} symmetry or a geometry very near to this ideal symmetry in the mentioned compounds. The O–O bond length has values between 134.$_5$ (K^+)[1] and 128.$_5$ pm ($N(CH_3)_4^+$),[4] while the O(2)–O(1)–O(3) bond angle varies between 113.$_5$ and 119.$_5$°.

O_3^- centers doped into various host structures as $KClO_3$,[6] MgO,[7] and KCl[8] or stabilized in an argon matrix[9] as well as in liquid ammonia[10,11] have been postulated and spectroscopically characterized already in a series of papers. Thus, a second aim of this study is the comparison of our data with the results in the literature. A very recent review gives the present status of the ozonide research in solid-state chemistry.[12]

Experimental Section

Because ozonides are thermodynamically metastable and extremely sensitive to moisture and carbon dioxide,[12] they were sealed in glass capillary tubes under dry argon. $N(CH_3)_4O_3$ is more stable ($T_{dec} \approx 75$ °C) than $N(C_2H_5)_4O_3$ and the alkali-metal ozonides,[12] which slowly decompose already at room temperature.

The EPR experiments were performed with a Varian E15 spectrometer at Q-band frequency (35 GHz) at 298 K [$N(CH_3)_4O_3$ single crystal] and 130 K. DPPH ($g = 2.0036$) was used as an internal standard. Uncertainties of the *g* values are estimated to be ±0.0015. For the single-crystal investigations the orientations of the crystallographic axes have been determined by X-ray methods. The crystals of RbO_3 and $N(CH_3)_4O_3$, sealed in glass capillaries, were then orientated visually with respect to the magnetic field direction.

Unpolarized optical absorption spectra of platy KO_3, RbO_3, and $N(CH_3)_4O_3$ single crystals were measured with a Beckman MS 1206 microspectrophotometer in the range 5000–35 000 cm^{-1}. Zeiss Ultrafluars 10× were used as the condenser and objective. As a light source served an Osram 450-W xenon lamp; the detector in the 5000–13 000-cm^{-1} range was a cooled P 2682-01 (Hamamatsu) PbS cell. The diameter of the measuring aperture was 0.06 mm. The spectral bandwidth of the visible region was 5×10^{-6} mm. So far only unpolarized spectra could be measured, because the intensity of the transmitted light was rather low due to the thickness of the crystals. Although the spectra were taken at 298 K, no decomposition of the crystals occurred during the measurement.

EPR Results

$N(CH_3)_4O_3$. Because the orthorhombic unit cell contains only two O_3^- anions, which are magnetically equivalent, this compound was selected first for a single-crystal EPR study (298 K). The angular dependence of the *g* values is shown in Figure 1. It is immediately seen that the g-tensor components follow the crystallographic *a*, *b*, and *c* axis within 10°. This angle should be considered as the experimental error due to the uncertainty in adjusting the crystal (enclosed in a glass capillary) in the magnetic field and in the determination of the *g* values (±0.0015). The best fit *g* values, derived from the data underlying Figure 1, are $g_a = 2.017$, $g_b = 2.007$, and $g_c = 2.009$. The powder spectrum at 130 K (Figure 2), which is not fully resolved, yields the approximate *g* values 2.018, 2.005, and 2.011—in good agreement with the single-crystal results. The principal *g* values were assumed to correspond to the maximum, the minimum, and the basis line transition of the signal, respectively. Simulations did not give better results, because the ratio between the *g* anisotropy (measured in gauss) and the line width is only about 1. The line width of the EPR signal varies between 45 and 68 G depending on the magnetic field direction.

The orientation of the g-tensor components with respect to the symmetry elements of the O_3^- anions with (approximate) C_{2v} geometry is easily accessible in this case. The molecular C_2 axis is oriented parallel to the crystallographic *c* axis, while *b* has the direction of the normal to the molecular plane. With the chosen coordinate system, *x*, *y*, *z* for the O_3^- entity in Figure 3 (following the convention in ref 6) the molecular g-tensor components have to be assigned as follows: $g_x = 2.007$, $g_y = 2.017$, and $g_z = 2.009$.

MO_3 ($M = K^+$, Rb^+, Cs^+, $N(C_2H_5)_4^+$). The compound RbO_3 is monoclinic with two pairs of magnetically inequivalent O_3^- anions in the unit cell, whose orientations deviate strongly from the directions of the crystallographic axes. Only one signal is observed in the single-crystal experiment, however, and the main *g* values follow the crystallographic axes: *g* (parallel to *b*) ≈ *g* (parallel to *a*) = 2.008, *g* (parallel to *c**) = 2.013 (130 K). Obviously, the g tensor is exchange-narrowed and can be reproduced with the molecular *g* values $g_x = 2.004$, $g_y = 2.016$, and $g_z = 2.009$, and the orientational angles of the two O_3^- radicals

† Dedicated to Prof. Dietrich Babel on the occasion of his 60th birthday.
‡ Philipps-Universität.
§ Universität Bonn.

(1) Schnick, W.; Jansen, M. *Rev. Chim. Miner.* **1987**, *24*, 446.
(2) Schnick, W.; Jansen, M. *Z. Anorg. Allg. Chem.* **1986**, *532*, 37.
(3) Jansen, M.; Hesse, W. *Z. Anorg. Allg. Chem.* **1988**, *560*, 47.
(4) Hesse, W.; Jansen, M. *Angew. Chem.* **1988**, *100*, 1388.
(5) Hesse, W.; Jansen, M. Manuscript in preparation.
(6) Schlick, S. *J. Chem. Phys.* **1972**, *56*, 654.
(7) Wong, N.-B.; Lunsford, J. H. *J. Chem. Phys.* **1972**, *56*, 2664.
(8) Callens, F.; Matthys, P.; Boesman, E. *J. Phys. C: Solid State Phys.* **1988**, *21*, 3159.
(9) Jacox, M. E.; Milligan, D. E. *J. Mol. Spectrosc.* **1972**, *43*, 148.
(10) Solomon, I. J.; Hattori, K.; Kacmarek, J.; Platz, G. M.; Klein, M. J. *J. Am. Chem. Soc.* **1962**, *84*, 34.
(11) Giguère, P. A.; Herman, K. *Can. J. Chem.* **1974**, *52*, 3941.
(12) Hesse, W.; Jansen, M.; Schnick, W. *Prog. Solid State Chem.* **1989**, *19*, 47.

0020-1669/91/1330-1923$02.50/0

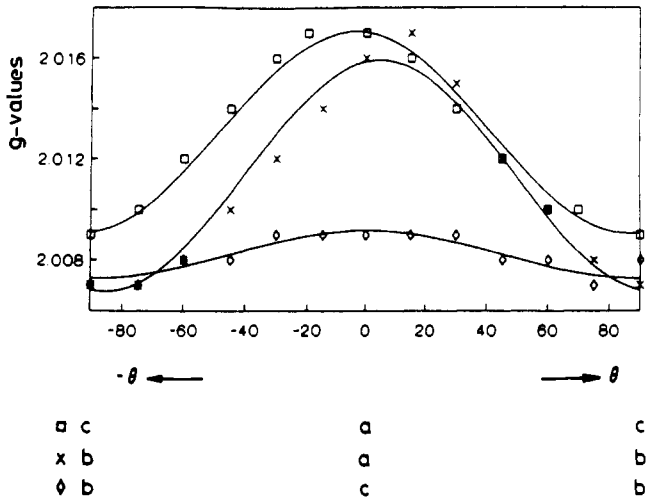

Figure 1. Angular dependence of the g values of $N(CH_3)_4O_3$ at 298 K, 35 GHz, with the magnetic field rotated in the (001), (010), and (100) planes.

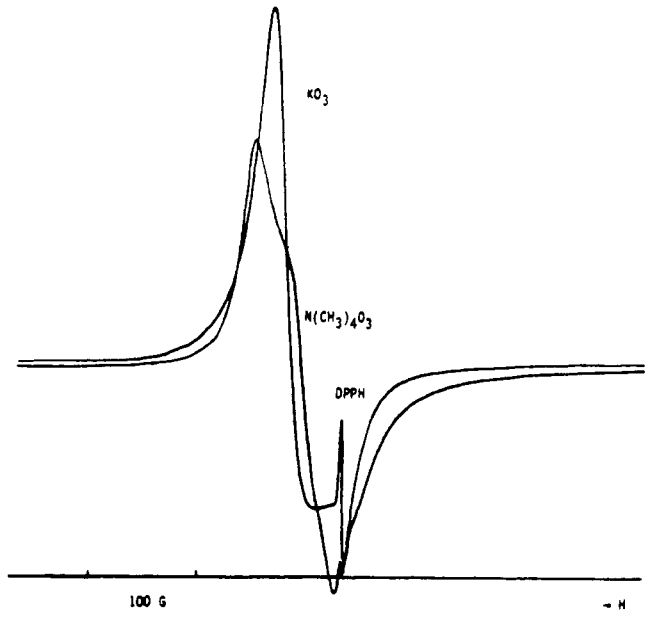

Figure 2. EPR powder spectra (130 K, 35 GHz) of compounds MO_3.

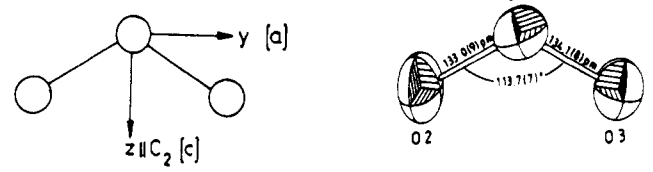

Figure 3. Left: Orientation of the **g**-tensor components and optical axes for compounds MO_3. The directions of the crystallographic axes are also indicated for $M = N(CH_3)_4^+$ (x and b are orientated perpendicular to the molecular plane). Right: Geometry of the O_3^- radical anion in RbO_3[2].

with respect to the crystallographic axes, in an analogous way as outlined below for the simpler case of KO_3. The signal line width varies between 65 and 90 G, depending on the magnetic field direction. Because the difference between the exchange-coupled g values is small in relation to the observed line width, only a nonresolved isotropic signal at $g \approx 2.009$ is observed in the powder spectrum.

The EPR powder spectrum of KO_3 is tetragonal with $g_\parallel^{ex} \approx 2.004$ and $g_\perp^{ex} \simeq 2.014$. The g values were approximated as the minimum and maximum positions of the EPR signal. As outlined in the following subsection, the spectrum is also controlled by

Table I. EPR Line Widths (G; Estimations from Powder Spectra in Parentheses[a]), Calculated Second Moments (Square Roots; G), and Neel Temperatures (K) and Curie–Weiss Constants (K) for Ozonides MO_3

	K^+	Rb^+	Cs^+	$N(CH_3)_4^+$	$N(C_2H_5)_4^+$
ΔH_{pp} (130 K)	(<65)	65–90	(≈340)	45–68[b]	(<75)
$(M_2^d)^{1/2}$	530	500	430	195	80
T_N[15,16]	20	17	6	<4	<4
θ[15,16]	−34	−23	−10	−5	≈0

[a] The given upper limits include the effects of the g anisotropy. [b] 298 K.

exchange interactions (Figure 2). The tetragonal unit cell contains eight O_3^- anions, which represent only two magnetically inequivalent orientations 1 and 2, however. With utilization of the results for $N(CH_3)_4O_3$ with respect to the orientation of the g components to the molecular symmetry elements (Figure 3, left), the analysis on the basis of the structural data yields that g^1_x and g^2_x are aligned parallel to the crystallographic [001] direction, while g^1_y, g^1_z and g^2_y, g^2_z are located in the (001) plane with the canting angle $2\gamma = 90°$ between $g^1_{y(z)}$ and $g^2_{y(z)}$. In such a case the molecular g values are related to the exchange-narrowed values by eq 1.[13] With $\gamma = 45°$ a tetragonal **g** tensor with the components $g_\parallel^{ex} = g_x$ and $g_\perp^{ex} = {}^1/_2(g_y + g_z)$ indeed results. From the observed g^{ex} values molecular g values of $g_x = 2.004$, $g_y \simeq 2.018$, and $g_z \simeq 2.010$ are deduced, if one considers 2.018 as the upper limit for g_y.

$$g_c^{ex} = g_x \qquad g_b^{ex} = (\cos^2\gamma)g_z + (\sin^2\gamma)g_y$$
$$g_a^{ex} = (\sin^2\gamma)g_z + (\cos^2\gamma)g_y \tag{1}$$

The spectrum of $N(C_2H_5)_4O_3$ is very similar to the one of $N(CH_3)_4O_3$ with the same average g value. The powder spectrum of CsO_3 shows a very broad signal at $g_{av} = 2.006$ with a rather high line width of 340 G (see next subsection).

EPR Line Width and Exchange Interactions. In the case of small distances between the O_3^- anions in the unit cell, exchange narrowing may occur, which obscures the molecular g values, if magnetically inequivalent paramagnetic centers are present.

The exchange field should strongly depend on the distances between the O_3^- radicals and hence on the ionic radii of the M^+ cation in the various ozonides. We have calculated the second moments M_2^d of the dipolar interaction, which are related to the dipolar broadening of isotropic EPR powder signals:[14]

$$M_2^d = {}^3/_5 g^2\beta^2 S(S+1)\sum_{j=1}^{\infty} 1/r_{jk}^6 \qquad (M_2^d)^{1/2} \approx \Delta H_{pp} \tag{2}$$

Here β is the Bohr magneton and r_{jk} the spacing between the jth and kth spin. For the sake of simplicity we have assumed that the unpaired electron is localized on the central oxygen atom of the ozonide anion and have neglected interactions beyond 700 pm. Though the results are only rather crude estimates, they are helpful to qualitatively understand the line-broadening mechanism in dependence on the M^+ countercation. As expected, the square roots of the second moments decrease with increasing M^+ radius (Table I). Because the EPR line width is determined by dipolar broadening *and* exchange narrowing, the comparison of the observed line width with the second moments should indicate whether significant exchange effects, even leading to exchange averaging of the **g** tensor, are present or not. Apparently exchange interactions are very small for cations larger than Rb^+. The line width seems to be predominantly due to dipolar broadening, as is clearly seen by the increase of ΔH_{pp} switching from the alkylammonium salts to CsO_3 (Table I). The enhancement is much stronger than

(13) Ozarowski, A.; Reinen, D. *Inorg. Chem.* **1985**, *24*, 3860.
(14) Poole, Ch. P. *Electron Spin Resonance*; Interscience Publishers: New York, 1967; Chapter 20K, p 836 ff.
(15) Lueken, H.; Deussen, M.; Jansen, M.; Hesse, W.; Schnick, W. *Z. Anorg. Allg. Chem.* **1987**, *553*, 179.
(16) Lueken, H.; Deussen, M.; Jansen, M.; Hesse, W. Manuscript in preparation.

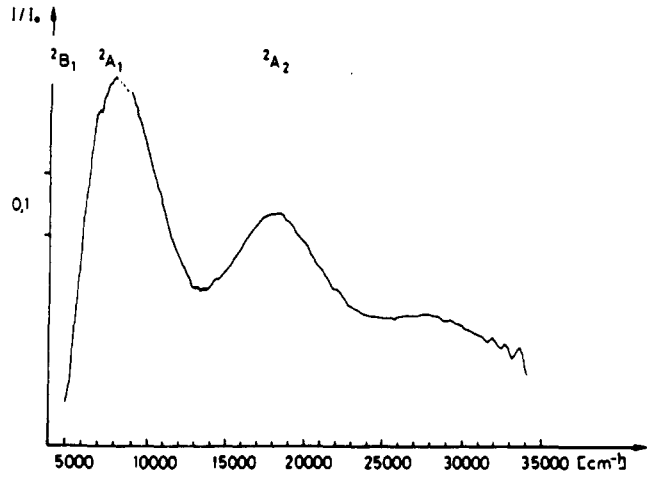

Figure 4. Unpolarized transmission spectrum of a single crystal of $N(CH_3)_4O_3$ of platy habitus (0.5 × 0.25 mm) measured in the (001) plane at 298 K.

expected from the second moments, however, presumably caused by lattice imperfections connected with the phase transition of CsO_3 at 281 K. The comparison of the single-crystal line width and the $(M_2^d)^{1/2}$ values of $N(CH_3)_4O_3$ and RbO_3 is particularly enlightening. Pure dipolar effects predict a line broadening by a factor of ≈2.5, while only a line-width increase of about 50% is actually observed—a clear indication of the presence of exchange effects.

These findings are in agreement with comparatively high antiferromagnetic ordering temperatures $T_N \approx 20$ K and Curie–Weiss constants $|\Theta|$ of rubidium and potassium ozonide (Table I). They also nicely match with the observation of an exchange-narrowed **g** tensor in these cases. Already small exchange fields are sufficient to average the g values, because the magnetic field difference, which determines the anisotropy of the **g** tensor, is tiny.

Results of Optical Spectroscopy

The color of the single crystals varies from brownish red (KO_3, RbO_3) to orange-red ($N(CH_3)_4O_3$) and is due to the minimum between the two bands at 8000 and 18 500 cm^{-1} and the transparency in the blue-violet region of the visible spectrum (Figure 4). The band positions do not vary significantly with the M^+ cation. The higher energy band was observed before for the O_3^- ion in solid $KClO_3$ and $NaClO_3$ matrices[17] as well as in liquid ammonia[10,11] but at the considerably higher energy of 22 000 cm^{-1}. The lower energy band has not been reported so far.

A tentative assignment of the spectrum is proposed on the basis of the various published MO schemes for the O_3^- radical.[18,19] In all diagrams the highest occupied molecular orbitals are those originating from the nonbonding π_g and antibonding π_u^* molecular orbitals of the hypothetical linear anion, which are $2b_2$, $1a_2$ and $2b_1^*$, $3a_1^*$, respectively (Figure 5). They only differ in the energetic position of the $3a_1^*$ molecular orbital, which strongly depends on the O(2)–O(1)–O(3) bond angle and is sometimes calculated to have an energy lower than the one of $1a_2$ (always for an angle of 116°).[18] On the basis of the orbital sequence in Figure 5, the following ground and lowest energy excited states (spin doublets only) result:

$$\begin{array}{llllll} \ldots\ldots & (1a_2)^2 & (2b_2)^2 & (3a_1^*)^2 & (2b_1^*)^1 : & {}^2B_1 \\ \ldots\ldots & (1a_2)^2 & (2b_2)^2 & (3a_1^*)^1 & (2b_1^*)^2 : & {}^2A_1 \\ \ldots\ldots & (1a_2)^2 & (2b_2)^1 & (3a_1^*)^2 & (2b_1^*)^2 : & {}^2B_2 \\ \ldots\ldots & (1a_2)^1 & (2b_2)^2 & (3a_1^*)^2 & (2b_1^*)^2 : & {}^2A_2 \end{array} \quad (3)$$

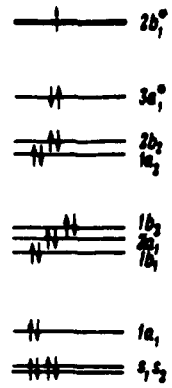

Figure 5. MO scheme for the orbital sequence of ClO_2 and O_3^- after Walsh.[20]

From the three possible transitions only those from $^2B_1 \rightarrow {}^2A_1$ and $\rightarrow {}^2A_2$ are symmetry-allowed in C_{2v} with the electrical dipole vector along x and y (Figure 3), respectively. The $^2B_1 \rightarrow {}^2B_2$ transition is vibrationally allowed parallel to x by the coupling to the vibrational β_2 mode. The three normal vibrations of the symmetries α_1 (2×) and β_2 are observed at ≃1010 (symmetric stretch ν_1), ≃620 (symmetric deformation ν_2) and ≃820 cm^{-1} (asymmetric stretch ν_3).[21] From the observed progressions in the band around 22 000 cm^{-1} of the ClO_2 and similarly of the O_3^- radical, it was concluded that it corresponds to the $^2B_1 \rightarrow {}^2A_2$ rather than to the $^2B_1 \rightarrow {}^2A_1$ transition.[9] The latter band was predicted to occur at about 10 000 cm^{-1} for ClO_2,[22] which is indeed very close to our findings (Figure 4). There is some indication of a very weak band around 28 500 cm^{-1} with no obvious assignment (Figure 4).

The results of an ab initio (CASSCF + CI) calculation of the O_3^- term diagram, which is performed in order to assign more conclusively the optical transitions as deduced from optical single-crystal spectra, will be published separately.[23]

Summary and Conclusions

The measured molecular g components of the O_3^- anion in the various ozonides MO_3 are $g_x = 2.006$ (2), $g_z = 2.010$ (1), and $g_y = 2.017$ (1) and vary only within the experimental error limits. A dependence on the specific O_3^- geometry is apparently not present, which matches with calculations indicating that even changes of 15° and 0.1 Å affect the g values only slightly ($\delta g_y \approx \delta g_z \approx 0.002$).[24]

The EPR spectra of O_3^- radicals, generated by irradiation of oxygen-17-enriched $KClO_3$ and trapped in the lattice, have been measured by Schlick.[6] The close similarity of the derived g values ($g_x = 2.004$, $g_y = 2.019$, $g_z = 2.012$) with those reported here and the equivalence of the orientation of the **g**-tensor components (Figure 3) give the final proof that the observed paramagnetic centers were indeed O_3^- entities. Nearly the same g values are also observed for O_3^- centers in KCl.[8] The magnetic moments of the O_3^- entities (1.74 μ_B)[15] are in accord with the spin-only value and an average g-value of 2.01.

The unpaired electron resides in the $2b_1$ molecular orbital with the wave function

$$\Psi_g = -c_1 p_x^1 + c_2(p_x^2 + p_x^3)/\sqrt{2} \quad (4)$$

The coefficients have been calculated from the O^{17} hyperfine structure in the EPR signal of O_3^--doped $KClO_3$[6] to be $c_1 \simeq c_2 \simeq 0.8$, which value implies that the electron density is about equally divided between the central O(1) atom and the two O(2), O(3) atoms.

(17) Bates, J. B.; Pigg, J. C. *J. Chem. Phys.* **1975**, *62*, 4227.
(18) Atkins, P. W.; Symons, M. C. R. *The Structure of Inorganic Radicals*; Elsevier: Amsterdam, 1967.
(19) Cremer, D. *The Chemistry of Functional Groups, Peroxides*; J. Wiley: New York, 1983.
(20) Walsh, A. D. *J. Chem. Soc.* **1953**, 2266.
(21) Karelin, A. I.; Rosolovskii, V. Ya.; Tokareva, S. A.; Vol'nov, I. I. *Dokl. Akad. Nauk SSSR* **1972**, *206*, 641.
(22) Humphries, C. M.; Walsh, A. D.; Warsop, P. A. *Discuss. Faraday Soc.* **1963**, *35*, 137.
(23) Koch, W.; Frenking, G.; Steffen, G.; Assenmacher, W.; Reinen, D. Manuscript in preparation.
(24) Mikheikin, I. D.; Zhidomirov, G. M.; Chuvylkin, N. D.; Kazanskii, V. B. *J. Struct. Chem.* **1974**, *15*, 678.

The unpolarized single-crystal spectra exhibit two bands at 8000 and 18 500 cm^{-1}, which are tentatively assigned to the $^2B_1 \rightarrow {}^2A_1$ and $^2B_1 \rightarrow {}^2A_2$ transitions, respectively. The lower energy band has not been observed before, while the second band appears at about 22 000 cm^{-1} for O_3^--doped solids and in solution. The large shift of about 3500 cm^{-1} for the higher energy band is very surprising, because the O-O bond length and O(3)-O(1)-O(2) bond angles of the O_3^- centers in $KClO_3$ (128 pm and 120 ± 6°, as estimated from CNDO calculations[6] on the basis of the EPR results) are very close to those found for the MO_3 compounds. Possibly strong matrix strains in case of the O_3^--doped host structures and solvent effects in liquid ammonia produce the considerable energy changes with respect to the MO_3 compounds, in which the O_3^- radicals are in a more or less unstrained state.

Contribution from the Department of Chemistry, McGill University, 801 Sherbrooke Street West, Montreal, Quebec H3A 2K6, Canada

Disulfanido Ligands:[1] Preparation and Reactions of $Cp_2Ti(SSR)X$, Where X = SR, Phthalimido, and Cl and R = Alkyl and Aryl Groups

Alan Shaver* and Stephen Morris[2]

Received September 4, 1990

The complex $Cp_2Ti(CO)_2$ oxidatively adds RSSX to give the complexes $Cp_2Ti(X)(SSR)$, where X = SR and R = $CHMe_2$, CMe_3, CH_2Ph, and 4-C_6H_4Me; X = phthalimido and R = $CHMe_2$, CMe_3, CH_2Ph, and 4-C_6H_4Me; and X = Cl and R = CPh_3. The complexes $Cp_2Ti(SR)(SSR)$ reacted with $PhCH_2Br$ to give $CpTiBr_2$, $PhCH_2SR$, and $PhCH_2SSR$, confirming the presence of the disulfanido ligand. These complexes desulfurized slowly in solution and rapidly in the presence of PPh_3 to give $Cp_2Ti(SR)_2$ and $SPPh_3$. The complexes for which X = phthalimido undergo alcoholysis to give the species where X = OET.

Introduction

While organic disulfides are common and are of industrial and biological importance, complexes containing terminal disulfanido ligands of the type RSS^- are rare and their chemistry relatively unknown. Nevertheless, a handful of such species have recently appeared. An (alkyldisulfanido)copper(II) species[3] was isolated from model studies of copper(II) enzymes (type A[3-8]). Model

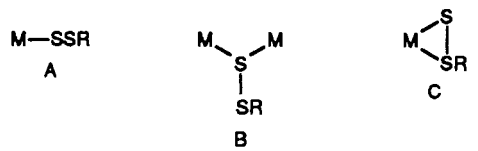

studies of molybdenum dimers by Nobel and co-workers[9a] gave complexes containing bridging disulfanido ligands (type B[9-12]). Similar bridging systems have also been observed in the anion[10] $[Fe_2S(SS\text{-}t\text{-}Bu)(CO)_6]^-$ and in the complexes $Cp_2Ti(\mu\text{-}SR)(\mu\text{-}SSR)Mo(CO)_4$, where R = $CHMe_2$ and CMe_3.[12] The complex $CpW(NO)(CH_2SiMe_3)(\eta^2\text{-}SSCH_2SiMe_3)$, which results from insertion of sulfur atoms[13] into the tungsten carbon bond, has a "side-on" bonding mode,[13c] which has also been observed in other systems (type C[13-15]). We have prepared the complexes $CpW(CO)_2SSR$[5,6] and *cis*-$(PPh_3)_2Pt(phth)SSR$,[5,7] where phth = phthalimido, which have simple terminal disulfanido ligands. The former spontaneously desulfurized in solution to give the corresponding thiolate while the latter was very stable. The complexes $Cp_2Ti(SSR)_2$, where R = aryl, rearrange to give $Cp_2Ti(SR)(SSSR)$; one of the first examples of a trisulfanido ligand.[8] The complexes $Cp_2Mo(SSR)_2$ extrude[16] the disulfide RSSR to give

Table I. Products of Oxidative Addition of RSSSR to $Cp_2Ti(CO)_2$[a]

	% product		
R	$Cp_2Ti(SSR)(SR)$	$Cp_2Ti(SR)(SR)$	$Cp_2Ti(SSR)(SSR)$
4-C_6H_4Me	84	16	0
$CHMe_2$	93	3	4
CMe_3	96	4	0
CH_2Ph	81	14	5

[a] Percentage, based on NMR integration of the peaks due to Cp and/or R groups at the point in the reaction when all $Cp_2Ti(CO)_2$ was consumed, as determined by IR.

(1) The IUPAC convention for linear polysulfur compounds is that they be named polysulfanes: Loening, K. L. In *Sulfur in Organic and Inorganic Chemistry*; Senning, A., Ed.; Marcel Dekker: New York, 1972; Vol. 3, pp 339-354.
(2) Present address: B.P. Chemicals Ltd., P.O. Box 21, Bo'ness Rd., Grangemouth, Stirlingshire FK3 9XH, United Kingdom.
(3) John, E.; Bharadwaj, P. K.; Krogh-Jespersen, K.; Potenza, J. A.; Schugar, H. J. *J. Am. Chem. Soc.* **1986**, *108*, 5015.
(4) Bhattacharyya, S. N.; Senoff, C. V.; Walker, F. S. *Inorg. Chim. Acta* **1980**, *44*, L273.
(5) Shaver, A.; Hartgerink, J.; Lai, R. D.; Bird, P.; Ansari, N. *Organometallics* **1983**, *2*, 938.
(6) Shaver, A.; Hartgerink, J. *Can. J. Chem.* **1986**, *65*, 1190.
(7) Shaver, A.; Lai, R. D. *Inorg. Chem.* **1988**, *27*, 4664.
(8) Shaver, A.; McCall, J. M.; Bird, P. H.; Ansari, N. *Organometallics* **1983**, *2*, 1894.
(9) (a) Nobel, M. E.; Williams, D. E. *Inorg. Chem.* **1988**, *27*, 749. (b) Nobel, M. E. *Inorg. Chem.* **1987**, *26*, 877. (c) Nobel, M. E. *Inorg. Chem.* **1986**, *25*, 3311.
(10) Wu, X.; Bose, K. S.; Sinn, E.; Averill, B. A. *Organometallics* **1989**, *8*, 251.
(11) Eremenko, I. L.; Pasynskie, A. A.; Kalinnikov, V. T.; Struchkov, Y. T.; Aleksandrov, G. G. *Inorg. Chim. Acta* **1981**, *52*, 107.
(12) Shaver, A.; Morris, S. Unpublished results.
(13) (a) Legzdins, P.; Rettig, S. J.; Sánchez, L. *Organometallics* **1988**, *7*, 2394. (b) Legzdins, P.; Sánchez, L. *J. Am. Chem. Soc.* **1985**, *107*, 5525. (c) Evans, S. V.; Legzdins, P.; Rettig, S. J.; Sánchez, L.; Trotter, J. *Organometallics* **1987**, *6*, 7.
(14) (a) Clark, G. R.; Russel, D. R. *J. Organomet. Chem.* **1979**, *173*, 377. (b) Hoots, J. E.; Rauchfuss, T. B. *Inorg. Chem.* **1983**, *22*, 2806. (c) Leonard, K.; Plute, K.; Haltiwanger, R. C.; Rakowski-Dubois, M. *Inorg. Chem.* **1979**, *18*, 3246.
(15) For examples of cyclic ligands containing the catenated S_2 unit, see: (a) Halbert, T. R.; Pan, W.-H.; Stiefel, E. I. *J. Am. Chem. Soc.* **1983**, *105*, 5476. (b) Giolando, D. W.; Rauchfuss, T. B. *Organometallics* **1984**, *3*, 487. (c) Giolando, D. W.; Rauchfuss, T. B.; Rheingold, A. L.; Wilson, S. R. *Organometallics* **1987**, *6*, 667. (d) Coucouvanis, D.; Lippard, S. J. *J. Am. Chem. Soc.* **1971**, *91*, 307. (e) Fackler, J. D.; Fetchin, J. A.; Fries, D. C. *J. Am. Chem. Soc.* **1972**, *94*, 7323. (f) Coucouvanis, D. *Prog. Inorg. Chem.* **1979**, *26*, 301.

0020-1669/91/1330-1926$02.50/0